D.Hasterok, M.Gard, G.Cox, M.Hand

A 4 Ga record of granitic heat production: Implications for geodynamic evolution and crustal composition of the early Earth

Precambrian Research, 2019; 331:1-14

Final publication at http://dx.doi.org/10.1016/j.precamres.2019.105375

A 4 Ga record of granitic heat production: Implications for geodynamic evolution and crustal composition of the early Earth

D. Hasterok[a,b,*], M. Gard[a], G. Cox[a], M. Hand[a,b]

[a]*Department of Earth Sciences, University of Adelaide, North Terrace, SA, 5005, Australia*
[b]*Mawson Centre for Geoscience (MCG), University of Adelaide, North Terrace, SA, 5005, Australia*

Abstract

The radiogenic heat produced by granites has a significant influence on the thermal state of the crust due to both their relatively high heat production with respect to most rock types and high abundance. However, the variations in present day heat production with age are generally based on relatively few measurements that are poorly distributed geographically. In this study, we construct a global model for the heat production of granitic rocks for the past 4 Ga using 13,400 geochemical analyses. We observe a nearly monotonic increase in radiogenic heat production from 4.0 to 2.0 Ga, which mirrors a shift from more TTG-like calcic to more alkalic compositions. This shift towards high-heat-producing granites post-2.0 Ga is often attributed to enrichment related to reworking and/or erosion. However, there is a strong correlation between granitic heat production with that of similarly-aged basalts and gabbros, which suggests a dominant mantle-level component to granite generation rather than crustal reworking. Secular cooling and mantle depletion may affect heat production, but the signal is complex and cannot easily explain the heat production with age profile. The most likely mechanism to describe the observed heat production–age pattern is one of selective preservation as a consequence of thermal stability. High heat producing terranes that were not stable during the Archean become increasingly stable towards the present. This selective preservation model has significant implications for the growth and composition of the continental crust. Ferroan, alkalic and felsic compositions were less thermally stable in the Archean due to their generally higher heat production and thus may have been more common in the early Earth than assumed by most compositional models. The temporal heat production model determined in this study can be used to improve geotherm models, particularly within ancient terranes.

Keywords: radiogenic heat generation, continental lithosphere, granite, crustal composition, Precambrian geodynamics

*Corresponding author

Email addresses: dhasterok@gmail.com (D. Hasterok), matthew.gard@adelaide.edu.au (M. Gard), grant.cox@adelaide.edu.au (G. Cox), martin.hand@adelaide.edu.au (M. Hand)

1. Introduction

Variations in radiogenic heat production distributions affect crustal temperatures, thus impacting a number of important Earth processes including metamorphism and magmatism, buoyancy, deformation due influences on crustal strength, thermal maturation of petroleum, and the melting and viscosity of ice sheets (Sandiford et al., 2001; Kelsey and Hand, 2015; Hasterok and Gard, 2016; Goodge, 2018; Zhang et al., 2019). As a result, it is necessary to improve our understanding of the lithologic variations in heat production, not just in space, but in time as well. Such a temporal record may also shed light on the changing chemical and physical geodynamic evolution of the crust and/or mantle.

Variations in heat flow within Precambrian terranes can largely be attributed to differences in heat production (Jaupart et al., 2016; Hasterok and Gard, 2016); though heat flow measurements are limited in many Precambrian regions (Davies and Davies, 2010; Goutorbe et al., 2011). Temporal models of upper crustal heat production for common crustal rocks are therefore necessary to improve models of Precambrian crustal temperatures and modeling lithospheric evolution. Since heat production is derived from heat producing elements (HPEs) that are typically incompatible during melting, there is also a potential to improve models for the chemical evolution of the continental crust. Granites are an ideal lithology to study these processes because they represent a significant fraction of the heat generated by internal radioactive decay of HPEs within the continental crust. This dominance is largely due to the considerably higher average heat production of felsic plutonic rocks coupled with their relatively high abundance in the upper crust (Rudnick and Gao, 2003; Hasterok and Webb, 2017; Artemieva et al., 2017).

Previous temporal models of heat production all suggest lower heat production during the Archean relative to the present (Vitorello and Pollack, 1980; Nyblade, 1999; Jaupart et al., 2016; Artemieva et al., 2017). Regional models similarly suggest lower Archean heat production (Kukkonen and Lahtinen, 2001; Slagstad, 2008). There are several processes that may contribute to a lower Archean heat production or higher heat production in post-Archean granites:

1. fundamental shifts in the sources, conditions and/or processes leading to granite genesis

(Condie, 2013; Laurent et al., 2014);

2. erosional removal of high-heat-producing upper crust exposes deeper low-heat-producing layers within older terranes (Vitorello and Pollack, 1980);

3. reworking by partial melting of continental crust refines and enriches younger granitic melts in older lithosphere (Condie, 1989);

4. secular cooling results in an increase in heat production as melt fractions decrease towards the present (Hawkesworth et al., 2010); and

5. increased thermal stability of low-heat-producing terranes results in a higher probability of survival (selective preservation), particularly during the Archean when Earth's interior was hotter (Morgan, 1985; Sandiford and McLaren, 2002).

Since each of these processes are largely independent, it is possible that any or all of these processes are responsible for the temporal variations in heat production. It may be possible in some cases to estimate their importance on heat production based on additional chemical indicators or the exact nature of heat production variations.

It is difficult to assess the importance of the above hypotheses from existing heat production models. Vitorello and Pollack (1980) and Jaupart and Mareschal (2014) estimate temporal variations in heat production from surface heat flow constraints, but there are several limitations to this method. First, the crustal heat production contribution is subject to complex lithologic variations (Hasterok and Webb, 2017; Hasterok et al., 2018), which likely obscures the processes discussed in the hypotheses above. Second, assigning a crustal age can be difficult because of the complexity of crustal formation and reworking, requiring such studies to use very large age bounds that severely limit the precise timing and nature of any temporal heat production variations and potentially alias tectonic processes. Third, uncertainties in mantle heat flow and lateral transport of heat add uncertainty to the heat production estimates. Artemieva et al. (2017) is the only study that focuses on a single lithology (granites) and uses gamma-ray spectral estimates of heat production, negating the first and third limitations of surface heat flow-based models. But the number of samples utilized in their analysis is small (<500), resulting in poor temporal resolution with significant spatial bias.

In this study, we develop a global model of heat production for granites with rock formation ages spanning 4 Ga to the present. The model is derived from a compilation of 24,555 whole rock geochemical analyses (13,400 with interpreted rock formation ages). We explore the compositional variations that lead to these variations in heat production. We present two basic temporal models of heat production that are independent of process but can be used to identify a deficit created by geodynamic processes that will affect heat production through time. We focus on thermal stability, which best explains the temporal heat production record and speculate on what this may mean for crustal compositions in Earth's early evolution.

2. Geochemical database

The 24,555 granitic samples utilized in this study are extracted from a global geochemical dataset comprised of ∼841,000 whole rock analyses with data. Many of the data have been extracted from the EarthChem databases (EarthChem.org, 2016), OzChem (Champion et al., 2016), and Petlab (Strong et al., 2016) databases, which are supplemented with publicly available technical reports, country and provincial databases, and peer-reviewed publications. The peer-reviewed publications target geographic regions and periods of time poorly sampled by the larger databases and account for nearly half the age-constrained data.

To ensure a consistent definition for the granites analyzed by this study, we first normalize the composition to anhydrous conditions, and then use the total alkali-silica (TAS) plutonic classification scheme by Middlemost (1994) to determine the rock type. Though granites are typically classified using a QAP scheme, very few of the geochemical samples include modal mineralogy with the records. Both plutonic and metaplutonic samples of granitic composition are combined for analysis in this study as recent studies have suggested there is a negligible effect of metamorphism on heat production (Slagstad, 2008; Hasterok et al., 2018; Alessio et al., 2018).

The locations of granites discussed in this study are shown in Figure 1. The full database contains 24,555 granites for which heat production can be estimated, 54% of the samples (13,400) are reported with an age resolution/bound of less than ±200 Ma (Supplemental Figure 1). The vast majority of the data (>80%) have a reported uncertainty < ±50 Ma). The whole-rock analyses, metadata, computed properties and additional descriptions of the dataset construction are provided in the Supplementary Material. While approximately half the granite analyses have reported or estimated ages, we use the remaining granitic data to explore potential spatial and temporal biases in the temporally constrained data that are the subject of this study.

3. Methods

The heat production for individual samples is computed using K, Th, and U concentrations by

$$A(\mu\text{W m}^{-3}) = \rho(9.52\,C_{\text{U}} + 2.56\,C_{\text{Th}} + 2.89\,C_{\text{K}_2\text{O}}) \times 10^{-5}, \tag{1}$$

where ρ is the sample density and C is the concentration of each respective heat-producing element (HPE); both U and Th are in ppm and K_2O is in weight percent (Rybach, 1988).

The HPEs concentrations are included from each whole rock analysis, but density is rarely measured and therefore must be estimated. Many geochemical and gamma-ray spectroscopy studies assume densities for known rock types; typically, 2600 to 2700 kg m^{-3} for granite (Artemieva et al., 2017). However, density may also be estimated from the major element geochemistry based on thermodynamic calculations (Hasterok and Webb, 2017) or by constructing a regression model fit to samples with known chemistry and density (Hasterok et al., 2018). Both methods yield similar uncertainties, although the thermodynamic model must be shifted by a constant to result in an equivalent mean to the regression model, possibly a result of minor porosity or fractures in the measured samples.

To estimate density, we use the empirical relationship developed by Hasterok et al. (2018)

$$\rho = 2532 + 216\,\text{Fe}^* + 608\,\text{maficity} - 10.0\,\text{MALI} \tag{2}$$

where

$$\begin{aligned}
\text{Fe}^*\ \text{(iron number)} &= C_{\text{FeO}_\text{T}}(C_{\text{FeO}_\text{T}} + C_{\text{MgO}})^{-1} \\
\text{MALI (modified alkali-lime index)} &= C_{\text{Na}_2\text{O}} + C_{\text{K}_2\text{O}} - C_{\text{CaO}} \\
\text{maficity} &= n_{\text{Fe}} + n_{\text{Mg}} + n_{\text{Ti}},
\end{aligned}$$

where n is the molar fraction (Frost et al., 2001; Clemens et al., 2011). This relationship is based on an analysis of geochemical variations within igneous samples with density estimates that are included in the database (Haus and Pauk, 2010; Bédard et al., 2016; Barette et al., 2016; Slagstad, 2008, 2017). Estimated 1-σ uncertainty for this density model is ± 91 kg m^{-3}, resulting in a heat production uncertainty for each sample of $\sim$3%. We consider this uncertainty acceptable and better than simply assuming a constant density for all samples.

The distribution of granitic heat production is fit considerably better by a log-normal distribution than a Gaussian. We believe this is an important point given that many studies still apply Gaussian statistics to heat production distributions despite gamma-ray spectra (Artemieva et al., 2017, Figures 8 and 13 to 15) and geochemical observations which imply otherwise (e.g. Ahrens, 1954; Rudnick et al., 1998; O'Neill and Jenner, 2012; Hasterok and Webb, 2017). While trends determined using Gaussian statistics are unlikely to differ, the magnitudes of the variations are likely to change. In addition to the magnitude, the accurate estimation of uncertainty/natural variability of distributions used to model subsurface temperatures will be incorrect. A Gaussian standard deviation fit to these data will have a 1- or 2-σ value that falls below 0—a non-sensical result (Figure 2).

For discussion of heat production throughout this paper, we frequently use the scale parameters (μ, σ) determined for a log-normal fit to the data, which represent the mean and standard deviation in log-space. In linear space, μ is equivalent to the median of the distribution, (i.e., the median is $\exp(\mu)$). However, for plotting data, we display either the distribution itself, or quantiles from this distribution so that significant deviations from log-normality may be assessed.

3.1. Sampling bias

A detailed assessment of bias is provided in the Supplementary Material whereas a brief summary is provided here.

The compilation of a geochemical dataset free from potential bias is difficult to achieve due to the large number of variables that must be considered. For instance, ideal sampling would cover all geographic regions in proportion to their spatial area within each time interval. Proper sampling must also ensure proportional sampling of the diverse array of terrane types, compositions, and histories. Therefore, a model completely free of bias even with more sophisticated sampling is unlikely. Keller and Schoene (2012) in their assessment of temporal changes in basaltic chemistry suggest creating a record of random sampling the same number of points from each geographic region to mitigate such biases. However, their method presents the potential to add bias by placing too great a weight on regions with a few samples at or below the number of random samples chosen from each region. As a result, these samples are be chosen every realization and if they deviate significantly from the global median, they could bias the record. Their method also fails to account for more complex factors such as terrane type and geologic history. We have therefore chosen a different approach, to identify regions of oversampling and assess them for deviations from median heat production. We do not remove them from the analysis but use this knowledge to aid our interpretation of the temporal model.

The sample locations are generally well-distributed around the continents (Figure 1), but there are obvious gaps in Russia, Central and Eastern Asia, and Africa. Some regions are extremely well-sampled with respect to much of the world, i.e., the United States and Australia. Most of the United States data are Phanerozoic in age and therefore will not affect the majority of the temporal record (Figure 1). However, this oversampling only provides a bias if the heat production of the oversampled regions is systematically above or below the global average. The North American data do not appear to deviate significantly from the global mean when accounting for relative area and therefore may not bias the record significantly.

4. Results and Discussion

4.1. Heat production–age model

Our estimated present-day heat production for a global set of granites as a function of crystallization age are shown in Figure 3a and presented in Table 1. From this model, we identify a few noteworthy observations: a general increase in heat production of granites from the Archean to 2.0 Ga; a step increase in heat production of granites at 2.0 Ga; and a high mid-Paleoproterozoic to early Mesoproterozoic heat production anomaly, which is due to high Australian heat production. A second (preferred) heat production–age model produced without the Australian samples results in generally lower heat production that is nearly constant from 2.0 Ga to the present (Figure 3). To understand why heat production of granites vary in time, it is necessary to know how evolving granite compositions relate to heat production.

4.2. Heat production–age and evolving granite composition

It is difficult to establish a direct relationship between heat production and crustal or mantle sources, which leads us to examine heat production variations with respect to a granite classification based on geochemical indices that are source agnostic yet demonstrate systematic variations with heat production. While the source composition is important, it is often very difficult to identify the source of granites because they can be derived from the relatively extreme end of the fractionation spectrum and large volumes can easily be derived from the mantle or crust or a composite of both (Moyen, 2019). Trace elements are often used to help identify the source, but they can also be difficult to interpret because similar patterns may arise from a variety of processes (Moyen, 2009). Thus, given the large diversity of granites incorporated in this study, making definitive statements about the source of "average" granites relatively meaningless. Therefore, we use a granite classification system by Frost et al. (2001) which makes no explicit assumptions about the source or tectonic environment, though some generalizations can be made. The classification system is based on three major element indices: iron number (Fe*); modified alkali-lime index (MALI); and alumina saturation index (ASI)).

The temporal variations in heat production of granites correlate with the chemical evolution of the average granite composition (Figure 4). Heat production of igneous rocks increases systematically as Fe* and MALI increase (Figure 8 in Hasterok and Webb, 2017). These trends typically indicate that heat production of granites increases as melts become more fractionated or reflects such a characteristic in the source. However, heat production exhibits no systematic change with respect to ASI, indicating that the presence or absence of metasediments in the source exert little influence on average heat production (Figure 8 in Hasterok and Webb, 2017).

Relative variations in ferroan to magnesian granites account for most of the average heat production variations in the Proterozoic and Phanerozoic. The median heat production of ferroan (high Fe*) granites is >1 μW m^{-3} greater than the median of magnesian granites (Figure 4c), which is consistent typically with a lower degree of crustal input into magnesian granites. The variations in the relative proportion of ferroan to magnesian granites matches the pattern of variations in heat production observed from 2.8 Ga to the present with only two age bins that do not fit the pattern. Whereas the general pattern seems to match the relative ferroan proportion, the magnitude cannot be easily determined by applying a simple scaling

(Figure 4a and c). These deviations are due to the natural variability of heat production among samples derived from a diverse set of source compositions, contaminants, and magma processes that may not lend themselves well to a consistent average behavior through time (i.e., large σ's in Figure 4c and d as a function of granite type).

The rise in median heat production through the Archean correlates with a decrease in the prevalence of magnesian-calcic granites (Figure 4b and d). The connection between the trends in ferroan proportion and heat production variations breaks down in the Archean and Paleoproterozoic but is consistent with a general increase in crustal input towards the present. Instead the Archean pattern of heat production correlates with a gradual shift in alkalinity from calcic to alkali-calcic granites (Figure 4b). In present day magmatic systems, magnesian-calcic granites are often associated with island arc plutonism (Frost et al., 2001). However, in the Archean these compositions more likely represent prevalence of trondhjemite-tonalite-granodiorite (TTG) forming processes (Condie, 2013; Laurent et al., 2014).

The lower heat production among magnesium-calcic granites and their greater prevalence in the Archean contribute to the 10 to 20 mW m^{-2} lower surface heat flow observed in Archean terranes today. This observation supports the compositional evolution hypothesis discussed in the introduction, but it does not necessarily preclude the remaining hypotheses as a cause of some degree of these compositional variations as discussed below.

4.3. A step change in average heat production?

Previous studies of temporal variations in heat production estimated independently using gamma-ray spectra and/or heat flow constraints (Nyblade and Pollack, 1993; Jaupart et al., 2016; Artemieva et al., 2017) indicate an increase in heat production between the Archean and Proterozoic, but the coarseness of temporal resolution of the previous studies place a step at the Archean–Proterozoic boundary (e.g. Figure 2). These larger time divisions place the heat production step 500 Ma too early whereas our uncertainty is the timing of the step is no more than $\pm$100 Ma. The model by Artemieva et al. (2017), based on a very small dataset, does resolve a step at a similar time but nearly all 24 Mesoproterozoic samples reside in Australia. Therefore, their dramatic step is mostly a consequence of high Australian heat production rather than a global phenomenon (Figure 3a).

At 2.0 Ga, there is a step increase in heat production to 2.59 μW m^{-3}. From 2.0 Ga to the present, the average heat production is ~2.6 μW m^{-3}, ranging from 2.2 to 2.9 μW m^{-3} excluding Australia and the Namaqua-Natal belt. To test for the statistical robustness of a step in heat production, we use Pettitt's test for a change point in a time series behavior (Pettitt, 1979). Without these data, the test identifies a possible change point in average granitic heat production at 2.0 Ga (p-value <0.0016) indicating a change in the average behavior before and after the step. A change point at 2.0 Ga is identified both with and without the Australian and Namaqua-Natal data.

Artemieva et al. (2017) suggest the increase in heat production during the Mesoproterozoic and subsequent decrease towards the present was associated with global models of average plate velocity by (Korenaga, 2006). They propose the higher velocities lead to increased frequency of continental collisions and greater volumes of granitic generation as a consequence. It is unclear how this mechanism leads to higher heat production as larger volumes of granitic generation probably originate from higher degrees of partial melting, which generally results in a decrease in heat production.

If collisions are ultimately the cause of high-heat-producing granites <2.0 Ga, then we would expect heat production variations to correspond with the tectonic cycle. Although the 2.0 Ga increase in granitic heat production coincides with the formation of the supercontinent Nuna, a lack of significant variations in average granitic heat production <2.0 Ga cannot be correlated to global tectonic cycles (Figure 3a and b). The 200 Ma bin size may alias the tectonic signal, but heat production variations at 100 Ma bin size (not shown) also do not correlate well with a tectonic cycle.

We suggest this step results from a rapid shift in the decrease in the depth of melting from a zone of garnet to plagioclase stability. This interpretation is evidenced by a step decrease in Sr/Y and La/Yb that occur at approximately the same time as the increase in heat production (Figure 8). It is difficult to discern whether this change is a gradual shift across a phase change or rapid shift in geodynamic processes. A more thorough geochemical analysis to explore the robustness, nature and cause of the step is presently underway (Hasterok et al., in prep).

4.4. High heat production anomalies

Perhaps the most striking features of the granitic heat production–age record in Figure 3a are the high heat production anomalies in the periods 2.0 to 1.4 Ga and 1.2 to 1.0 Ga. Heat production of mid-Paleoproterozoic to early Mesoproterozoic granites is >1 μW m^{-3} greater the Phanerozoic average. Artemieva et al. (2017) found a similarly high heat production among granites of this age (Figure 2), which the authors attributed to a peak in global increase in plate velocities. Though we suggest these peaks result from spatial bias rather than a global phenomenon.

Granites from Mesoproterozoic Australia (2.0 to 1.4 Ga) and the Namaqua-Natal belt (1.2 to 1.0 Ga) appear to be sources of significant high heat production anomalies (>1-σ from the mean) that bias the temporal record due to oversampling. The Namaqua-Natal belt is known for its high-heat-producing granites (Jones, 1987; Andreoli et al., 2006). Likewise, high median heat production in Australia is documented on both regional and outcrop scales from geochemistry and gamma-ray spectroscopy (Neumann et al., 2000; McLaren et al., 2005; Hasterok and Webb, 2017), heat flow (Chapman and Furlong, 1977; Morgan, 1985; Jaupart and Mareschal, 2007; McLaren et al., 2003), and thermal isostasy (Hasterok and Gard, 2016). Previous temporal studies of average heat production are generally aware of the high Australian heat production and exclude them as part of their analysis (Vitorello and Pollack, 1980; Jaupart et al., 2016). However, the recent granite heat production model by Artemieva et al. (2017) includes a significant fraction of Precambrian heat production estimates from Australia, particularly in the Mesoproterozoic. Although they mention the potential for geographic bias in their temporal model, they do not discuss the Australian anomaly as a source of their Mesoproterozoic high heat production.

A significant fraction (~70%) of the mid-Paleoproterozoic to early-Mesoproterozoic (2.0 to 1.4 Ga) samples in our dataset originate in Australia, which is higher heat-producing than the global average (Figure 3a). Likewise, nearly all of the samples from the Artemieva et al. (2017) model are from the high-heat-producing regions of Australia. Because Australian granites are over-represented in the dataset during this time period, we produce a global granitic model excluding these data (Figure 3a blue and Table 1). The heat production record produced from this reduced dataset is considerably lower without Australian data from 2.0 to 1.4 Ga and consistent with the heat production from 1.4 Ga to the present.

Compositionally, the Australian granites are more ferroan than general and while ferroan rocks do have median heat productions greater than the global average, there are other age bins with similarly high ferroan percentages (Figure 4). Therefore, it cannot be linked directly to the major element composition. The Th/U ratio of high-heat-producing Australian rocks are typical of most rocks, but the K/U ratio is low, suggesting an enrichment of U and Th with respect to K.

A common explanation for producing high-heat-producing granites is through multiple generations of partial melting, which assumes U and Th are preferentially partitioned into melts. The partial melting hypothesis requires that each subsequent melting step produce a smaller volume of high-heat-producing material. For high heat production terranes this model presents a problem, how to produce large volumes of high heat producing granites such as the Mesoproterozoic Australia and the Namaqua-Natal Belt (McLaren et al., 2003; Andreoli et al., 2006). Furthermore, the solubility of monazite—a Th rich mineral—is highly dependent on the presence of fluids during melting (Alessio et al., 2018). Under fluid absent conditions, the source rock may retain a significant portion of the heat-producing elements, or even increase in heat production, resulting in melts that are no more heat producing than the source (Alessio et al., 2018). Therefore, it is more likely that the sources from which these granites were extracted had high heat production themselves.

4.5. A deficit in Archean heat production

We present two basic models that are used as a reference with which to identify temporal heat production anomalies. These models are not meant to physically explain the variations in average heat production, but they are instead a convenient metric with which to identify heat production variations from geodynamic processes. Both models fit the heat production data relatively well over the past $\sim$2.0 Ga, but overpredict the heat production record in the Archean (Figure 3a and b). Both models are anchored to the median present-day heat production (2.63 μW m^{-3}) for granites 0.2 to 0 Ga with HPE concentrations 4.48 wt.%, 17.1 ppm and 4.24 ppm for K_2O, Th, and U, respectively.

The first and simplest model assumes the formation heat production of granites decay to a constant heat production at present (CHPP) irrespective of the formation age (Figure 3a). This model assumes the conditions of granite formation are effectively identical throughout the past, and that the source is not significantly depleted with time. The only temporal changes in source heat production are the result of radiogenic decay. The CHPP model assumes HPE concentrations are identical at present regardless of the formation age, which is not consistent with observations (Supplemental Figure 6).

The second model assumes a constant heat production at formation (CHPF) for granites (Figure 3a). This model assumes that K concentration is effectively constant among crystallizing granites and that K/U and Th/U concentrations are identical at the time of formation of granites regardless of age. Post crystallization, these ratios evolve to differences in the present-day ratios with age because of differences in half-lives of the individual radioisotopes. The CHPF model is consistent with the present-day K/U and Th/U observations as a function of formation age (supplemental Figure 6). The model also implies that either the source becomes more enriched with time—a non-sensical result—or that there is a steady decrease in the melt fraction that results in a greater fraction of HPEs entering the melt.

The root mean square (RMS) misfits are 0.29 μW m^{-3} for the CHPP model and 0.21 μW m^{-3} for the CHPF model from 2.0 to 0 Ga. The RMS increases for both models when heat production of bins >2.0 Ga are included in the calculation. The CHPF model is better than a simple linear fit to the heat production record over the same period (RMS, 0.22 μW m^{-3}).

Irrespective of which model is chosen as the reference, there is a deficit in heat production in the Archean (Figure 3b). Granitic heat production during the Archean is systematically lower than the Proterozoic and Phanerozoic. Despite relatively few samples (<100) within half of the Archean age bins, the median heat production across the bins shows a fairly consistent increase in heat production from the early Archean, 0.53 μW m^{-3}, to the Paleoproterozoic, 1.83 μW m^{-3}at $\sim$2.0 Ga (Figure 3a).

Our study is not the first to note an increase in heat production from the Archean to present (Vitorello and Pollack, 1980; Nyblade and Pollack, 1993; Jaupart et al., 2016; Artemieva et al., 2017), but our higher resolution model suggests heat production systematically increases from 4.0 to 2.0 Ga, allowing us to revisit these previous hypotheses described in the introduction.

In Figure 5, we summarize the trends of several temporally varying global geodynamic processes that are expected to have on heat production including erosion, reworking, depletion, secular cooling and thermal preservation. The net result of these processes must ultimately result in the pattern we observe today. Below we discuss the predictions and evidence for and/or against each of these processes as a significant contributor to the observed heat production.

Our initial focus is on the global pattern in heat production without anomalous regions such as Mesoproterozoic Australia and the Namaqua-Natal Belt.

4.5.1. Erosion

Heat-flow based models of crustal heat production predict an increase towards the present in an exponential, or similar, fashion. Vitorello and Pollack (1980) suggested the cause of this variation is the result of erosional removal of the high heat producing, felsic upper crust exposing lower heat producing, intermediate to mafic crust below. This model was founded on seismic velocity and geochemical models suggesting the continental crust becomes increasingly mafic with depth and heat production observations that display a general correlation between SiO_2 and heat production (e.g., Christensen and Mooney, 1995; Rudnick and Gao, 2003; Hasterok and Webb, 2017; Hasterok et al., 2018).

Erosion is most effective at reducing high elevation differences created as a result of tectonic and geodynamic process, but decreases in effectiveness as the surface is brought closer to level with surrounding regions (Montgomery and Brandon, 2002; Willenbring et al., 2013). The timescales for erosion of mountain belts are on the order of a few hundred million years (Fischer, 2002). Therefore, we expect the first-order, depth-of-erosion to produce a heat production–age pattern resembles an erosional decay curve with time (Figure 5 Vitorello and Pollack, 1980).

Because our heat production–age model is based on granites alone, it limits the influence of potentially large changes in lithology that would give rise to this temporal heat flow pattern. Although even among granites, there is an increase in heat production with SiO_2 (Figure 6a). Median granites on the upper end of the SiO_2 range have nearly twice as much heat production as median granites that sit on the lower end (Figure 6a). However, neither the median SiO_2 of granites through time nor the heat production–age record fit this simple erosional model (Figure 3a).

There are problems with this simplistic erosional model for temporal variations heat production. First, the average denudation is not monotonically increasing through time and many Archean terranes exhibit very little erosion, with typical level of exposure between greenschist to upper amphibolite metamorphic grade (Dewey, 2007). This observation suggests the pattern expected from erosion may be more complex, though undoubtedly some degree of erosion must occur to expose the granites we observe today. Second, recent studies suggest the generally increasing model of maficity with depth may not be accurate for all regions (Hacker et al., 2011; Williams et al., 2014; Hacker et al., 2015), thus SiO_2 may not decrease with depth in a systematic way.

There are variations in the average SiO_2 in granites between 72 and 75 wt.% with time, but these variations are not correlated with variations in heat production. Hence, the decrease in heat production of granites is unlikely to be due to erosion and must result from another process.

4.5.2. Reworking

There is abundant evidence for reworking as many igneous rocks contain inherited zircons. In addition, models of continental growth based on Nd and Hf isotopes also suggest crustal and mantle reworking are important processes in continental crustal evolution and may account for a significant fraction of the present continental crustal volume (Armstrong and Harmon, 1981; Condie and Aster, 2013; Dhuime et al., 2017; Spencer et al., 2017). Melting, as a consequence of reworking, is often assumed to increase the heat production of a melt relative to its source since the partition coefficients of HPEs in crystals to melts are often significantly less than 1. Since the heat production of sedimentary rocks are generally high (Hasterok et al., 2018), granites formed by partially melting sedimentary sources are generally expected to have higher heat production. Because reworked volumes increase during the formation of supercontinents (Hawkesworth et al., 2010; Condie and Aster, 2013), the pattern of heat production we expect should generally increase with time, with a possible superposition of a tectonic cycle that results in peaks in heat production when multiple generations of melting may occur producing extra enrichment during these periods (Figure 3c,d and 5).

We offer two observations that refute the reworking model with respect to the temporal variations in median granitic heat production. First, median heat production is fairly constant among granites with ages from 2.0 Ga to the present (Figure 3) suggesting a minimal influence of reworking. We may not observe a reworking effect despite many ancient regions experiencing multiple instances of metamorphism. Often, the first metamorphic event is lower temperature, perhaps thermally buffered by melting. The second metamorphic event can then progress to higher temperatures, but it may not produce melts as the melt potential was exhausted in the first instance of metamorphism (e.g., Morrissey et al., 2016). Hence, the redistribution of heat production due to reworking is likely to happen once in a given terrane. Since temporal variations in heat production do not show a clear reworking signal, it is useful to examine whether the typical assumption that partial melting of crustal sources produces an increase in heat production is justified. The existence of inherited zircons in granitic melts suggest that they do not fully dissolve in the source rock during melting either because the rate of melt production is too rapid (Bea et al., 2007), or the partition coefficients are not significantly less than 1. The solubility of zircon and monazite, major accessory minerals that contain a significant fraction of U and Th, are highly dependent on the temperature and fluid characteristics during melting (Rapp and Watson, 1986; Ayers and Watson, 1991; Montel, 1993). Under fluid absent conditions, the source rock may retain a significant portion of the heat producing elements, possibly even increasing in heat production (Alessio et al., 2018). Thus reworking does not necessarily deplete old crust or enrich young crust.

The second observation that contradicts a simple reworking signal expressed in temporal changes in median heat production is a strong correlation between mafic samples and granites with similar crystallization dates (Figure 7a). We interpret this correlation as an indication of the importance of a mantle-derived component to the majority of granites. While this correlation may not completely exclude reworking of mafic crust (e.g., remelting of a growing mafic underplate), such a correlation requires that the reworking be nearly contemporaneous with the formation of the mafic crust and not reworking of significantly older crust. It should be noted that the spatial distribution of granites and basalts/gabbros in this analysis are not in perfect correspondence, implying that this influence represents a global phenomenon and not simply a local effect resulting from crustal contamination of mafic magmas. Samples older than 3.2 Ga do not fit the granite/basalt heat production trend, but this may be due to the relatively few samples and limited localities from which these data are drawn or as a disconnect between their respective processes of melt generation.

4.5.3. Secular cooling, mantle depletion and HPE concentrations

During partial melting of the mantle, partition coefficients for HPEs between the mantle residue and basaltic melt are <1 (Workman and Hart, 2005). As a result, higher degrees of partial melting will result in lower heat production than low degrees of partial melting. Since mantle temperatures were higher in the Archean (Herzberg et al., 2007; Condie et al., 2016), it is reasonable to assume that melt fractions generated in the Archean would have been high and heat production of mafic crust similarly low, though this neglects changes in source fertility that are addressed later. We expect granites generated by fractional or partial melting of these mafic materials are low heat producing simply because they started with low heat production. As the Earth undergoes secular cooling, melt fractions are expected to fall resulting in an increase in heat production through time.

While the exact nature of the cooling of the mantle is subject to debate, both Herzberg et al. (2007) and Condie et al. (2016) estimate relatively stable mantle temperatures in the Archean transitioning to a rapid decrease in temperatures starting in the Meso- to Paleoproterozoic and continuing to the present. The initially slow cooling of the Earth should produce high degrees of partial melt with relatively low and constant heat production in the early Earth. Then as mantle temperatures begin to fall more rapidly, the decrease in partial melt should result in heat production that continues to rise until the present day in a pattern similar to that shown in Figure 5.

The pattern of observed heat production is not what is expected from a purely secular cooling model (Figure 3a and 5). However, one cannot separate the increased volumes of melt produced during the Archean from the depletion of HPEs in the mantle. For the same degree of partial melting, the temporal effect of depletion on heat production will result in higher Archean heat production than at present (Figure 5 Grigné and Labrosse, 2001). Therefore, a signal from secular cooling should take this into account, and the net effect will be a combination of the temperature and depletion effects (Figure 5). However, this signal could be quite complicated since the influence of melt fraction on concentration follows a power-law relationship and depletion is additionally dependent on the volumes of crustal growth and subduction erosion. Modeling the coupled secular cooling–mantle depletion process is beyond the scope of this study. Some studies suggest that the vast majority of mantle depletion had occurred prior to 3.52 Ga, or even pre-3.8 Ga (Jacobsen and Dymek, 1988; Galer and Goldstein, 1991; Bowring and Housh, 1995). In this case, the effect of depletion is effectively negligible on heat production and the secular cooling signal should be rather simple (Figure 5).

Regardless, we expect the secular cooling effect to be generally greater than the effect of depletion since depletion has a nearly linear effect on the heat production of melts extracted from the mantle whereas the effect of melt fraction is a power-law relationship with an increasingly large effect as melt fraction decreases. The effect of secular cooling should be greatest at near the present and depletion greatest in the early Earth.

Despite the challenges in modeling the nature of heat production resulting from a coupled secular cooling–mantle depletion process, we can investigate its potential as the cause of the observed heat production pattern by examining chemical proxies associated with melting. Higher crustal temperature gradients in the past would suggest that the granite solidus would likely be reached at shallower crustal depths. The Sr/Y ratio is often considered a proxy for the depth of melting as an increase in Sr/Y indicates a greater fraction of plagioclase relative to garnet dissolved in the melt, i.e., higher pressure where garnet is stable (Defant and Drummond, 1990). One may assume that the increase in pressure on a global scale is indicative of a lower geothermal gradient. The La/Yb ratio is another possible chemical proxy that can be used for the secular cooling and La/Yb ratios are typically higher in low degrees of partial melting and therefore are expected to rise as Earth cools.

While the Sr/Y ratio over the past <2.0 Ga is lower compared with the prior 2.0 Ga, the relatively rapid decrease in Sr/Y at ~ 2.0 Ga is inconsistent with the slowly changing expectation from secular cooling (Figure 8a). Likewise, La/Yb ratios also predict lower melt fractions >2.0 Ga, further suggesting cooler conditions during melting of granite sources in the early Earth. Secular cooling may still affect heat production through other mechanisms such as thermal preservation, but a direct effect does not appear to be the dominant process controlling the heat production pattern with age.

4.5.4. Thermal stability and selective preservation

We are not the first to suggest selective preservation as mechanism to describe the chemical distribution of rocks that remain from the Archean. However, most of these studies rely on tectonic mechanisms (Condie, 1990; Hawkesworth et al., 2010; Ault et al., 2015). Selective preservation as a result of thermal stability does not require any specific tectonic mechanism for survival (Morgan, 1985). Relatively low thermal stability results from the higher lithospheric temperatures of high-heat-producing terranes, which increases the probability of reworking—particularly when buried (Sandiford et al., 2002). This process differs from the reworking hypothesis in that high-heat-producing terranes need not be the product of enriched partial melts, but these terranes are high heat producting simply because their sources started with high heat production.

The heat production we observe today of Archean granites is much lower than it initially started due the subsequent decay of HPEs (Table 2). As a result, the temperature contribution of HPEs to crust was much greater in the Archean terranes of the past (Figure 9. Since radioactive decay reduces HPEs exponentially with time, regions with heat production equivalent to what was high in the Archean become increasingly stable towards the present (Morgan, 1985). As a consequence, we expect the heat production pattern arising from selective preservation by way of thermal stability to result in a pattern, at present, of increasing heat production that rapidly rises through the Archean-aged terranes and increases more slowly through the Proterozoic to the present (Figure 5).

The high-heat-producing terranes of Australia are an anomalous region of thermally weak crust, which illustrates how thermal reworking occurs. The burial of Australian high-heat-producing rocks likely weakened the central Australian lithosphere sufficiently to permit intracrustal orogens (Hand and Sandiford, 1999; McLaren et al., 2006). When buried, these terranes may raise crustal temperatures sufficiently to recrystallize and reset igneous ages or melt the crust. Had plate boundary forces not changed or the deformation proceeded more rapidly, it is possible the Australian crust would have been reworked. While the magnitude of heat production found in Australian granites is not unprecedented, the volume of such crust within a single region is highly unusual (Supplementary Figure 3).

We develop a possible survival model for the thermal preservation of low-heat producing Archean lithosphere. To compute this model, we require an estimate of geotherms for Archean terranes prior to and after preservation. Figure 9 shows geotherms computed assuming a distribution of upper crustal heat production equivalent to Archean granites, both at present and at 3.5 Ga. A similar set of geotherms are produced for the present-day granitic heat production distribution. Interestingly, the Archean geotherms at 3.5 Ga are statistically similar to the estimated lithospheric temperatures for 0.2 to 0 Ga (Figure 10a and Supplementary Material). Clearly there is a limit to how hot the crust can be before it will recrystallize or melt; therefore, we suggest this similarity is an indication that the present-day Archean heat production distribution was limited by thermal stability in the early Earth.

If we assume that the initial Archean heat production distribution was the same as the present-day heat production projected to the past, we can estimate the nature of the survival function required to produce the observed Archean heat production distribution. There are two methods we use to estimate the survival function using depths to an isotherm in the geotherm distributions. The first method directly computes the survival function by dividing the estimated initial Archean distribution by the surviving Archean distribution (i.e., B divided by D in Figure 10a). The second method estimates the survival function by a Gaussian cumulative distribution function (CDF) that when multiplied by the initial Archean distribution will produce the best fit to the observed Archean distribution (Figure 10). Complete details of the survival function modeling are given in the Supplemental Material.

Both methods yield similar survival probability functions (Figure 10b). However, the ratio method yields a much longer tail to shallower depths indicating that there is a small probability that some small high-heat-producing regions may be preserved. This extended tail is to be expected as tectonic forces may not always achieve the threshold sufficient to rework the crust or the high-heat-producing terranes may be too small to sufficiently heat and destabilize the crust. It may be within these anomalous regions that the compositions of destroyed crust may be determined, which are generally more ferroan and alkalic than the bulk of preserved rocks.

Though the survival functions predicted in this study (Figure 10b) and crustal-growth models (Figure 3d) are somewhat speculative, both can be used to estimate the volume of Archean crust that has survived. The predicted percentage of Archean crust preserved under this scenario represents $\sim$8.6% of the continental crust created during the Archean by integrating the survival ratio function over depth (light line, Figure 10). The estimated preservation volume can be determined by the ratio of the preserved crustal volume to the reworked or recycled crust (Figure 3d), which ranges from approximately 7 to 11% at 3.5 Ga. The similarity between these two estimates may add further support to a thermal stability hypothesis, and crustal growth models that incorporate reworking and recycling. We are not suggesting the volume of continental crust in the Archean was as high as the present at any given instant, but it was higher than what is preserved, which is consistent with continental growth models by Dhuime et al. (2017) and Spencer et al. (2017) (Figure 3d).

The correlation between basalt/gabbro and granite heat production does not rule out a selective survival mechanism (Figure 7). Many terranes show correlations between the heat production, seismic velocity and SiO_2 (Hasterok and Webb, 2017; Hasterok et al., 2018). Therefore, terranes with low granitic heat production that are likely to be thermally stable will also have lower mafic heat production, which may preserve the correlation between the two parameters at any given age (Figure 7b). But there are clear outliers to this trend in the early Archean with considerably higher mafic heat production (or lower felsic heat production) than expected. For two of these three deviations, the mafic heat production is anomalously high with respect to the mafic-felsic trend line (Figure 7a). Though still lower than similarly aged granites, crust that is dominantly mafic may still have relatively low heat production and therefore be more likely to be preserved. This selective preservation of mafic over felsic dominated crust could further bias the compositional distribution of present-day Archean crust.

Sedimentary rocks do not appear to record a the high-heat-producing crust, instead resulting in a Th and U record similar in nature to the Th and U concentrations through time for granites examined by this study (McLennan and Taylor, 1980). Sedimentary rocks, particularly shales, are often considered integrators of crustal composition (McLennan, 2001). Since sediments likely record some component of igneous rocks that no longer exist, we expect to find some sediments that record high-heat-producing terranes are preferentially destroyed. However, it is also possible that any high-heat-producing sedimentary rocks, if buried—a large fraction of Archean sediments are metamorphosed (McLennan and Taylor, 1980)—will be subject to similar thermal stability criteria as the igneous crust. As a result, sedimentary rocks containing a significant fraction of a higher heat producing source in the Archean may also have a low probability of survival. Furthermore, the average transport distance for sediments in the Archean was likely much shorter than today due to the smaller size of the crustal blocks, increasing the likelihood that the sediments would be sourced from igneous crust similar to that which was preserved. Indeed, many Archean sediments are volcaniclastic and there are very few shales suggesting short transport distances.

4.6. Implications of selective preservation on Archean crustal composition

If thermal instability of the crust due to high heat production in the Archean resulted in significant percentages of reworking, melting, etc., then the compositional evolution models of the early Earth must be reconsidered. We can expect the granites that were destroyed were more ferroan and alkalic since they are typically higher heat-producing than magnesian calcic granites (Figure 4). Therefore, TTG-like granites were a smaller fraction of the initial crust than what survived the Archean and the processes generating granites may have been more similar to today than previously thought. In addition, the higher heat production of felsic to intermediate crust would have an increased the probability of destruction. Felsic dominated crust is typically associated with thicker and more continental-type crust, making it additionally likely that it would be destroyed. A recent geochemical analysis of terrigenous sediments is consistent with our interpretation of a higher proportion of Archean felsic crust (Greber and Dauphas, 2019). Thus, portions of the Archean crust were thicker, more felsic, and thus higher elevation than previously thought.

Selective preservation also has implications for the thermal gradients associated with metamorphism. Brown and Johnson (2018) compiled estimates of metamorphic gradients from the present to 3.8 Ga and found fewer and lower magnitude high metamorphic thermal gradients in the Archean than the Proterozoic. The distribution of high metamorphic thermal gradients in the Archean are more similar to those today (Brown and Johnson, 2018, Figure 6). They attributed these lower thermal gradients during the Archean to a prevalence of vertical tectonics (bivergent subduction) rather than the more typical horizontal tectonics (asymmetric subduction) of the Proterozoic and Phanerozoic. We suggest the high geothermal gradients in the Archean were selectively destroyed, leaving only the lower magnitude high geothermal gradients.

The surviving Archean crust may be anomalous in Earth's history, but the crust that was reworked, remelted, or recycled may have been more similar to the Proterozoic than previously realized.

5. Conclusions

Granitic heat production has changed considerably over the past 4 Ga, generally increasing from the Archean to the present day. The granitic heat production variations are correlated with changes in the chemistry of granites, with more magnesian and calcic granites contributing to lower heat production during the Archean and more ferroan and alkalic granites contributing to higher heat production since the mid-Proterozoic. This transition likely indicates a shift away from TTG formation.

The increase of heat production in the Archean does not fit with temporal trends predicted by erosional or reworking processes. Erosion is particularly unlikely as the typical level of Archean crustal exposure is greenschist to upper amphibolite, not granulite grade as expected from the basic hypothesis. Secular cooling coupled with mantle depletion may contribute to a decrease in Archean heat production, but the expected pattern may be very complex because of mantle depletion and refertilization through continental erosion. Additionally, the estimated pressure of granites formed in the Archean is deeper than expected for a high geothermal gradient associated with a warmer Earth, perhaps indicating an upper limit to crustal temperatures.

The most likely mechanism that leads to an increase in heat production through the Archean and Paleoproterozoic is selective preservation as a result of thermal stability. Because of significantly lower heat production in the present due to radioactive decay, high-heat-producing terranes are more stable today than they would have been during the Archean. The surviving terranes may be chemically distinct from terranes that once existed. Because of the higher heat production among felsic, ferroan and alkalic compositions, the Archean may have had a greater relative proportion of these compositions than observed at present. Therefore, it may be necessary to include the chemical consequences of thermal stability into models of crustal growth and the chemical evolution of the silicate Earth.

A step increase in heat production occurs at 2.0 Ga, at which point heat production is relatively uniform to the present with the exception of two clear anomalous regions (Mesoproterozoic Australia and the Namaqua-Natal Belt of southern Africa). We suggest this step may be related to an increase in the average pressure at which granitic melts are produced. However, there is a paucity of granitic samples from 2.4 to 2.2 Ga so the step may not be a robust feature of the record. It is possible that this transition is more gradational occurring over a longer time interval.

A high mid-Paleoproterozoic to early Mesoproterozoic granitic heat production occurs within Australia and potentially biases the global average. Removing Australian granites results in a significantly lower heat production, which may or may not be anomalous depending on assumptions about the nature of the long-term heat production trends. Australian data should be included for calculations of the global heat budget or considered in temporal analyses of HPEs, but they should probably be excluded as a predictive tool for estimating heat production in unexplored regions except where these regions were joined to Australia when the continental growth occurred.

Only granites have been considered in this study. However, producing a global model of heat production through time requires that all rock types be considered, not just granites. Furthermore, future studies must consider the changing tectonic setting with time and related biases in the rock record. Although granites represent a significant fraction of the upper crust, the differences between heat production of granites and other rock types is greater than variations within granite alone (Hasterok et al., 2018); therefore, variations in crustal composition from one region to another have a potentially much larger influence on the total surface heat flow (Mareschal and Jaupart, 2013) and the thermal stability.

6. Acknowledgments

We would like to thank K. Condie, two anonymous reviewers, and editor V. Pease for their constructive comments that helped us improve the manuscript. We would like to thank the following individuals for providing datasets and/or personal compilations: D. Champion (GA) D. Claeson (SGU), T. Slagstad (NGU), and H. Furness. Peter Johnson provided a collection of papers with data for the Arabian-Nubian Shield. M. Gard is supported by Australian Government Research Training Program Scholarship. This research was supported partially by the Australian Government through the Australian Research Council's Discovery Projects funding scheme (project DP180104074). The views expressed herein are those of the authors and are not necessarily those of the Australian Government or Australian Research Council. This paper is Mawson Centre for Geoscience contribution XXXX.

Ahrens, L., 1954. The lognormal distribution of the elements (a fundamental law of geochemistry and its subsidiary). Geochimica et Cosmochimica Acta 5, 49–73. doi:10.1016/0016-7037(54)90040-X.

Alessio, K.L., Hand, M., Kelsey, D.E., Williams, M.A., Morrissey, L.J., Barovich, K., 2018. Conservation of deep crustal heat production. Geology 46, 335–338. doi:10.1130/g39970.1.

Andreoli, M., Hart, R., Ashwal, L., Coetzee, H., 2006. Correlations between U, Th content and metamorphic grade in the western Namaqualand Belt, South Africa, with implications for radioactive heating of the crust. J. Metamorphic Petrol. 47, 1095–1118. doi:10.1093/petrology/egl004.

Armstrong, R.L., Harmon, R.S., 1981. Radiogenic isotopes: The case for crustal recycling on a near-steady-state no-continental-growth earth [and discussion]. Philosophical Transactions of the Royal Society A: Mathematical, Physical and Engineering Sciences 301, 443–472. doi:10.1098/rsta.1981.0122.

Artemieva, I.M., Thybo, H., Jakobsen, K., Sørensen, N.K., Nielsen, L.S., 2017. Heat production in granitic rocks: Global analysis based on a new data compilation GRANITE2017. Earth-Science Reviews 172, 1–26. doi:10.1016/j.earscirev.2017.07.003.

Ault, A.K., Flowers, R.M., Bowring, S.A., 2015. Synchroneity of cratonic burial phases and gaps in the kimberlite record: Episodic magmatism or preservational bias? Earth and Planetary Science Letters 410, 97–104. doi:10.1016/j.epsl.2014.11.017.

Ayers, J.C., Watson, E.B., 1991. Solubility of apatite, monazite, zircon, and rutile in supercritical aqueous fluids with implications for subduction zone geochemistry. Philosophical Transactions: Physical Sciences and Engineering 335, 365–375. URL: http://www.jstor.org/stable/53707, doi:10.2307/53707.

Barette, F., Poppe, S., Smets, B., Benbakkar, M., Kervyn, M., 2016. Spatial variation of volcanic rock geochemistry in the Virunga Volcanic Province: Statistical analysis of an integrated database. Journal of African Earth Sciences doi:10.1016/j.jafrearsci.2016.09.018.

Bea, F., Montero, P., González-Lodeiro, F., Talavera, C., 2007. Zircon inheritance reveals exceptionally fast crustal magma generation processes in Central Iberia during the Cambro-Ordovician. Journal of Petrology 48, 2327–2339. doi:10.1093/petrology/egm061.

Bédard, J.H., Hayes, B., Hryciuk, M., Beard, C., Williamson, N., Dell'Oro, T.A., Rainbird, R.H., Prince, J., Baragar, W.R.A., Nabelek, P.I., Weis, D., Wing, B., Scoates, J., Naslund, H.R., Cousens, B., Williamson, M.C., Hulbert, L.J., Montjoie, R., Girard, É., Ernst, R., Lissenberg, C.J., 2016. Geochemical database of Franklin sills, Natkusiak Basalts and Shaler Supergroup rocks, Victoria Island, Northwest Territories, and correlatives from Nunavut and the mainland. Open-file 8009. Geological Survey of Canada. URL: https://doi.org/10.4095%2F297842, doi:10.4095/297842.

Bowring, S., Housh, T., 1995. The earth's early evolution. Science 269, 1535–1540. doi:10.1126/science.7667634.

Brown, M., Johnson, T., 2018. Secular change in metamorphism and the onset of global plate tectonics. American Mineralogist 103, 181–196. doi:10.2138/am-2018-6166.

Champion, D., Budd, A., Hazell, M., Sedgmen, A., 2016. OZCHEM National Whole Rock Geochemistry Dataset. Technical Report Downloaded July 2016. Geoscience Australia.

Chapman, D., Furlong, K., 1977. Continental heat flow/age relationships, in: EOS, Trans. Am. Geophys. Union, p. 1240 (abstract).

Christensen, N., Mooney, W., 1995. Seismic velocity structure and composition of the continental crust: a global view. J. Geophys. Res. 100, 9761–9788. doi:10.1029/95JB00259.

Clemens, J., Stevens, G., Farina, F., 2011. The enigmatic sources of I-type granites: The peritectic connexion. Lithos 126, 174–181. doi:10.1016/j.lithos.2011.07.004.

Condie, K.C., 1989. Geochemical changes in basalts and andesites across the Archean-Proterozoic boundary: Identification and significance. Lithos 23, 1–18. doi:10.1016/0024-4937(89)90020-0.

Condie, K.C., 1990. Geochemical characteristics of Precambrian basaltic greenstones, in:

Early Precambrian Basic Magmatism. Springer Netherlands, pp. 40–55. doi:10.1007/978-94-009-0399-9_3.

Condie, K.C., 2013. How to make a continent: Thirty-five years of TTG research, in: Modern Approaches in Solid Earth Sciences. Springer Netherlands, pp. 179–193. doi:10.1007/978-94-007-7615-9_7.

Condie, K.C., Aster, R.C., 2013. Refinement of the supercontinent cycle with Hf, Nd and Sr isotopes. Geoscience Frontiers 4, 667–680. doi:10.1016/j.gsf.2013.06.001.

Condie, K.C., Aster, R.C., van Hunen, J., 2016. A great thermal divergence in the mantle beginning 2.5 Ga: Geochemical constraints from greenstone basalts and komatiites. Geoscience Frontiers 7, 543–553. doi:10.1016/j.gsf.2016.01.006.

Davies, J., Davies, D., 2010. Earth's surface heat flux. Solid Earth 1, 5–24.

Defant, M.J., Drummond, M.S., 1990. Derivation of some modern arc magmas by melting of young subducted lithosphere. Nature 347, 662–665. doi:10.1038/347662a0.

Dewey, J.F., 2007. The secular evolution of plate tectonics and the continental crust: An outline, in: Geological Society of America Memoirs. Geological Society of America, pp. 1–7. doi:10.1130/2007.1200(01).

Dhuime, B., Hawkesworth, C.J., Delavault, H., Cawood, P.A., 2017. Continental growth seen through the sedimentary record. Sedimentary Geology 357, 16–32. doi:10.1016/j.sedgeo.2017.06.001.

EarthChem.org, 2016. Whole rock geochemistry data downloaded on June 10th. Technical Report. http://earthchem.org.

Fischer, K.M., 2002. Waning buoyancy in the crustal roots of old mountains. Nature 417, 933–936. doi:10.1038/nature00855.

Frost, B., Barnes, C., Collins, W., Arculus, R., Ellis, D., Frost, C., 2001. A geochemical classification for granitic rocks. J. Petrol. 42, 2033–2048. doi:10.1093/petrology/42.11.2033.

Galer, S., Goldstein, S., 1991. Early mantle differentiation and its thermal consequences. Geochimica et Cosmochimica Acta 55, 227–239. doi:10.1016/0016-7037(91)90413-y.

Goodge, J.W., 2018. Crustal heat production and estimate of terrestrial heat flow in central East Antarctica, with implications for thermal input to the East Antarctic ice sheet. The Cryosphere 12, 491–504. doi:10.5194/tc-12-491-2018.

Goutorbe, B., Poort, J., Lucazeau, F., Raillard, S., 2011. Global heat flow trends resolved from multiple geological and geophysical proxies. Geophys. J. Int. 187, 1405–1419. doi:10.1111/j.1365-246X.2011.05228.x.

Greber, N.D., Dauphas, N., 2019. The chemistry of fine-grained terrigenous sediments reveals a chemically evolved paleoarchean emerged crust. Geochimica et Cosmochimica Acta 255, 247–264. doi:10.1016/j.gca.2019.04.012.

Grigné, C., Labrosse, S., 2001. Effects of continents on earth cooling: Thermal blanketing and depletion in radioactive elements. Geophysical Research Letters 28, 2707–2710. doi:10.1029/2000gl012475.

Hacker, B.R., Kelemen, P.B., Behn, M.D., 2011. Differentiation of the continental crust by relamination. Earth and Planetary Science Letters 307, 501–516. doi:10.1016/j.epsl.2011.05.024.

Hacker, B.R., Kelemen, P.B., Behn, M.D., 2015. Continental lower crust. Annual Review of Earth and Planetary Sciences 43, 167–205. doi:10.1146/annurev-earth-050212-124117.

Hand, M., Sandiford, M., 1999. Intraplate deformation in central australia, the link between subsidence and fault reactivation. Tectonophysics 305, 121–140. doi:10.1016/s0040-1951(99)00009-8.

Hasterok, D., Gard, M., 2016. Utilizing thermal isostasy to estimate sub-lithospheric heat flow and anomalous crustal radioactivity. Earth and Planetary Science Letters 450, 197–207. doi:10.1016/j.epsl.2016.06.037.

Hasterok, D., Gard, M., Webb, J., 2018. On the radiogenic heat production of metamorphic, igneous, and sedimentary rocks. Geoscience Frontiers 9, 1777–1794. doi:10.1016/j.gsf.2017.10.012.

Hasterok, D., Webb, J., 2017. On the radiogenic heat production of igneous rocks. Geoscience Frontiers 8, 919–940. doi:10.1016/j.gsf.2017.03.006.

Haus, M., Pauk, T., 2010. Data from the PETROCH lithogeochemical database. Miscellaneous Release—Data 250. Ontario Geol. Surv.

Hawkesworth, C., Dhuime, B., Pietranik, A., Cawood, P., Kemp, A., Storey, C., 2010. The generation and evolution of the continental crust. Journal of the Geological Society 167, 229–248. doi:10.1144/0016-76492009-072.

Herzberg, C., Asimow, P., Arndt, N., Niu, Y., Lesher, C., Fritton, J., Cheadle, M., Saunders, A., 2007. Temperatures in ambient mantle and plumes: constraints from basalts, picrites, and komatiites. Geochem. Geophys. Geosys. 8, Q02006. doi:10.1029/2006GC001390.

Jacobsen, S.B., Dymek, R.F., 1988. Nd and Sr isotope systematics of clastic metasediments from Isua, West Greenland: Identification of pre-3.8 Ga differentiated crustal components. Journal of Geophysical Research: Solid Earth 93, 338–354. doi:10.1029/jb093ib01p00338.

Jaupart, C., Mareschal, J.C., 2007. Heat flow and thermal structure of the lithosphere, in: Shubert, G., Watts, A. (Eds.), Treatise on Geophysics: Crust and Lithospheric Dynamics. Elsevier. volume 6. chapter 5, pp. 217–251. doi:10.1016/B978-0-444-53802-4.00114-7.

Jaupart, C., Mareschal, J.C., 2014. Constraints on crustal heat production from heat flow data, in: Treatise on Geochemistry. Elsevier, pp. 53–73. doi:10.1016/b978-0-08-095975-7.00302-8.

Jaupart, C., Mareschal, J.C., Iarotsky, L., 2016. Radiogenic heat production in the continental crust. Lithos 262, 398–427. doi:10.1016/j.lithos.2016.07.017.

Jones, M., 1987. Heat flow and heat production in the Namaqua Mobile Belt, South Africa. J. Geophys. Res. 92, 6273–6289. doi:10.1029/JB092iB07p06273.

Keller, C.B., Schoene, B., 2012. Statistical geochemistry reveals disruption in secular lithospheric evolution about 2.5 Gyr ago. Nature 485, 490–493. doi:10.1038/nature11024.

Kelsey, D., Hand, M., 2015. On ultrahigh temperature crustal metamorphism: Phase equilibria, trace element thermometry, bulk composition, heat sources, timescales and tectonic settings. Geosci. Frontiers 6, 311–356. doi:10.1016/j.gsf.2014.09.006.

Korenaga, J., 2006. Archean geodynamics and the thermal evolution of Earth, in: Benn, K., Mareschal, J.C., Condie, K. (Eds.), Archean Geodynamics and Environments. Am. Geophys. Union. volume 164 of *Geophys. Monogr.* doi:10.1029/164GM03.

Kukkonen, I., Lahtinen, R., 2001. Variation of radiogenic heat production rate in 2.8–1.8 Ga old rocks in the central Fennoscandian Shield. Physics of the Earth and Planetary Interiors 126, 279–294. doi:10.1016/s0031-9201(01)00261-8.

Laurent, O., Martin, H., Moyen, J., Doucelance, R., 2014. The diversity and evolution of late-Archean granitoids: Evidence for the onset of 'modern-style' plate tectonics between 3.0 and 2.5 Ga. Lithos 205, 208–235. doi:10.1016/j.lithos.2014.06.012.

Mareschal, J.C., Jaupart, C., 2013. Radiogenic heat production, thermal regime and evolution of continental crust. Tectonophysics 609, 524–534. doi:10.1016/j.tecto.2012.12.001.

McLaren, S., Sandiford, M., Hand, M., Neumann, N., Wyborn, L., Bastrakova, I., 2003. The hot south continent: heat flow and heat production in Australian Proterozoic terranes, Geological Society of Australia. volume 22 of *Special Pub.*, pp. 151–161. doi:10.1130/0-8137-2372-8.157.

McLaren, S., Sandiford, M., Powell, R., 2005. Contrasting styles of Proterozoic crustal evolution: A hot-plate tectonic model for Australian terranes. Geology 33, 673–676. doi:10.1130/G21544AR.1.

McLaren, S., Sandiford, M., Powell, R., Newmann, N., Woodhead, J., 2006. Palaeozoic intraplate crustal anatexis in the Mount Painter Province, South Australia: Timing, thermal budgets and the role of crustal heat production. J. Petrol. 47, 2281–2302. doi:10.1093/petrology/egl044.

McLennan, S.M., 2001. Relationships between the trace element composition of sedimentary rocks and upper continental crust. Geochemistry, Geophysics, Geosystems 2, n/a–n/a. doi:10.1029/2000gc000109.

McLennan, S.M., Taylor, S.R., 1980. Th and u in sedimentary rocks: crustal evolution and sedimentary recycling. Nature 285, 621–624. doi:10.1038/285621a0.

Middlemost, E., 1994. Naming materials in the magma/igneous rock system. Earth Sci. Rev. 37, 215–224. doi:10.106/0012-8252(94)90029-9.

Miller, C.F., McDowell, S.M., Mapes, R.W., 2003. Hot and cold granites? implications of zircon saturation temperatures and preservation of inheritance. Geology 31, 529. doi:10.1130/0091-7613(2003)031<0529:hacgio>2.0.co;2.

Montel, J.M., 1993. A model for monazite/melt equilibrium and application to the generation of granitic magmas. Chemical Geology 110, 127–146. doi:10.1016/0009-2541(93)90250-m.

Montgomery, D.R., Brandon, M.T., 2002. Topographic controls on erosion rates in tectonically active mountain ranges. Earth and Planetary Science Letters 201, 481–489. doi:10.1016/s0012-821x(02)00725-2.

Morgan, P., 1985. Crustal radiogenic heat production and the selective survival of ancient continental crust. Journal of Geophysical Research 90, C561. doi:10.1029/jb090is02p0c561.

Morrissey, L.J., Hand, M., Kelsey, D.E., Wade, B.P., 2016. Cambrian high-temperature reworking of the Rayner—Eastern Ghats Terrane: Constraints from the Northern Prince Charles Mountains region, East Antarctica. Journal of Petrology 57, 53–92. doi:10.1093/petrology/egv082.

Moyen, J.F., 2009. High Sr/Y and La/Yb ratios: The meaning of the 'adakitic signature'. Lithos 112, 556–574. doi:10.1016/j.lithos.2009.04.001.

Moyen, J.F., 2019. Granites and crustal heat budget. Geological Society, London, Special Publications , SP491–2018–148doi:10.1144/sp491-2018-148.

Neumann, N., Sandiford, M., Foden, J., 2000. Regional geochemistry and continental heat flow: implications for the origin of the South Australian heat flow anomaly. Earth Planet. Sci. Lett. 183, 107–120. doi:10.1016/S0012-821X(00)00268-5.

Nyblade, A., 1999. Heat flow and the structure of Precambrian lithosphere. Lithos 48, 81–91.

Nyblade, A., Pollack, H., 1993. A global analysis of heat flow from Precambrian terrains: implications for the thermal structure of Archean and Proterozoic lithosphere. Journal of Geophysical Research: Solid Earth 113, 12207–12218. doi:10.1029/93JB00521.

O'Neill, H.S.C., Jenner, F.E., 2012. The global pattern of trace-element distributions in ocean floor basalts. Nature 491, 698–704. doi:10.1038/nature11678.

Pettitt, A.N., 1979. A non-parametric approach to the change-point problem. Applied Statistics 28, 126. doi:10.2307/2346729.

Rapp, R., Watson, E., 1986. Monazite solubility and dissolution kinetics: implications for the thorium and light rare earth chemistry of felsic magmas. Contributions to Mineralogy and Petrology 94, 304–316. doi:10.1007/bf00371439.

Rudnick, R., Gao, S., 2003. Composition of the continental crust, in: Rudnick, R. (Ed.), Treatise on Geochemistry: The Crust. Elsevier. volume 3. chapter 1, pp. 1–64. doi:10.1016/B978-0-08-095975-7.00301-6.

Rudnick, R., McDonough, W., O'Connell, R., 1998. Thermal structure, thickness and composition of continental lithosphere. Chem. Geology 145, 395–411. doi:10.1016/S0009-2541(97)00151-4.

Rybach, L., 1988. Determination of heat production rate, in: Hänel, R., Rybach, L., Stegena, I. (Eds.), Terrestrial Handbook of Heat-Flow Density Determination. Kluwer Academic Publishers, Dordrecht. chapter 4.2, pp. 125–142.

Sandiford, M., Hand, M., McLaren, S., 2001. Tectonic feedback, intraplate orogeny and the geochemical structure of the crust: a central Australian perspective, in: Miller, J., Holdsworth, J., Buick, I., Hand, M. (Eds.), Continental Reactivation and Reworking. Geol. Soc. London. volume 184 of *Spec. Pub.*, pp. 195–218.

Sandiford, M., McLaren, S., 2002. Tectonic feedback and the ordering of heat producing elements within the continental lithosphere. Earth Planet. Sci. Lett. 204, 133–150. doi:10.1016/S0012-821X(02)00958-5.

Sandiford, M., McLaren, S., Neumann, N., 2002. Long-term thermal consequences of the redistribution of heat-producing elements associated with large-scale granitic complexes. J. Metamorphic Geol. 20, 87–98.

Slagstad, T., 2008. Radiogenic heat production of Archean to Permian geological provinces in Norway. Norwegian Journal of Geology 88, 149–166.

Slagstad, T., 2017. LITO database (online): Geochemical mapping of Norwegian bedrock. Technical Report. Norges Geologiske Undersøkele (NGU). URL: `http://www.ngu.no/lito`.

Spencer, C., Roberts, N., Santosh, M., 2017. Growth, destruction, and preservation of Earth's continental crust. Earth-Science Reviews 172, 87–106. doi:`10.1016/j.earscirev.2017.07.013`.

Strong, D., Turnbull, R., Haubrock, S., Mortimer, N., 2016. Petlab: New Zealand's national rock catalogue and geoanalytical database. New Zealand J. Geol. Geophys. 53, 475–481. doi:`10.1080/00288306.2016.1157086`.

Vitorello, I., Pollack, H., 1980. On the variation of continental heat flow with age and the thermal evolution of the continents. J. Geophys. Res. 85, 983–995. doi:`10.1029/JB085iB02p00983`.

Willenbring, J.K., Codilean, A.T., McElroy, B., 2013. Earth is (mostly) flat: Apportionment of the flux of continental sediment over millennial time scales. Geology 41, 343–346. doi:`10.1130/g33918.1`.

Williams, M., Dumond, G., Mahan, K., Regan, S., Holland, M., 2014. Garnet-forming reactions in felsic orthogneiss: Implications for densification and strengthening of the lower continental crust. Earth and Planetary Science Letters 405, 207–219. doi:`10.1016/j.epsl.2014.08.030`.

Workman, R., Hart, S., 2005. Major and trace element composition of the depleted MORB mantle (DMM). Earth Planet. Sci. Lett 231, 53–72. doi:`10.1016/j.epsl.2004.12.005`.

Zhang, F., Jiao, Y., Wu, L., Rong, H., Li, J., Wan, D., 2019. Enhancement of organic matter maturation because of radiogenic heat from uranium: A case study from the Ordos Basin in China. AAPG Bulletin 103, 157–176. doi:`10.1306/06071817107`.

Table 1: Estimated global heat production through time.

formation age		All Data[a]								Excluding Australia[b]							
min	max	N	0.05	0.25	0.5	0.75	0.95	μ	σ	N	0.05	0.25	0.5	0.75	0.95	μ	σ
Ga			μW m^{-3}					ln (μW m^{-3})			μW m^{-3}					ln (μW m^{-3})	
0	0.2	3573	0.64	1.63	2.64	4.01	7.64	0.91	0.79	3554	0.63	1.62	2.63	4.01	7.65	0.91	0.79
0.2	0.4	1656	0.92	2.25	3.16	4.44	7.44	1.09	0.67	1331	0.77	2.13	2.91	4.14	6.72	1.00	0.69
0.4	0.6	3015	0.78	1.68	2.39	3.55	6.42	0.85	0.67	2968	0.78	1.67	2.39	3.55	6.28	0.85	0.67
0.6	0.8	503	0.53	1.58	2.67	4.61	7.90	0.89	0.94	445	0.49	1.48	2.41	3.95	7.27	0.77	0.93
0.8	1.0	215	0.59	1.17	2.24	3.51	7.32	0.71	0.80	215	0.59	1.17	2.24	3.51	7.32	0.71	0.80
1.0	1.2	289[c]	1.22	2.23	4.48	7.39	13.91	1.42	0.76								
1.0	1.2	202[d]	1.11	1.88	3.00	5.86	11.46	1.19	0.74	142[d]	1.07	1.71	2.83	5.48	13.29	1.16	0.78
1.2	1.4	70	0.96	2.07	2.79	4.36	6.73	0.99	0.63	69	0.95	2.09	2.87	4.38	6.75	1.00	0.62
1.4	1.6	468	1.29	2.75	3.97	7.24	12.54	1.43	0.73	133	1.06	1.66	2.46	3.41	5.90	0.90	0.65
1.6	1.8	756	1.10	2.88	4.15	6.39	11.93	1.39	0.72	182	0.56	1.49	2.43	4.15	9.84	0.91	0.90
1.8	2.0	1015	1.03	2.49	3.52	5.01	7.85	1.21	0.61	417	0.64	1.79	2.59	3.77	6.61	0.89	0.73
2.0	2.2	334	0.44	0.90	1.83	2.91	30.53	0.65	1.11	334	0.44	0.90	1.83	2.91	30.53	0.65	1.11
2.2	2.4	37	0.46	1.12	2.01	2.85	9.69	0.64	0.87	32	0.45	0.71	1.85	2.31	3.94	0.42	0.71
2.4	2.6	355	0.17	0.70	1.65	3.17	7.92	0.36	1.13	315	0.17	0.62	1.34	2.58	5.41	0.19	1.06
2.6	2.8	636	0.42	1.22	2.05	3.53	6.80	0.67	0.85	607	0.41	1.20	2.01	3.46	6.70	0.65	0.85
2.8	3.0	192	0.33	0.83	1.56	3.37	7.93	0.52	0.96	163	0.33	0.76	1.30	3.32	7.99	0.44	1.00
3.0	3.2	84	0.29	0.71	1.28	2.26	7.95	0.28	0.93	71	0.28	0.68	1.22	2.21	7.18	0.21	0.93
3.2	3.4	107	0.27	0.52	0.77	1.35	2.21	-0.20	0.64	102	0.27	0.51	0.74	1.30	2.26	-0.23	0.64
3.4	3.6	71	0.54	0.80	1.13	1.73	4.04	0.23	0.66	56	0.53	0.70	1.09	2.01	4.77	0.23	0.73
3.6	3.8	18	0.18	0.34	0.53	0.70	9.24	-0.51	1.07	18	0.18	0.34	0.53	0.70	9.24	-0.51	1.07
3.8	4.0	9	0.24	0.40	0.61	0.93	3.04	-0.43	0.78	9	0.24	0.40	0.61	0.93	3.04	-0.43	0.78
0	4.0	13400	0.61	1.68	2.72	4.22	8.15	0.94	0.81	11249	0.55	1.53	2.46	3.77	7.28	0.83	0.81
Global (all)[e]		24555	0.64	1.62	2.66	4.16	8.14	0.93	0.80	17826	0.55	1.45	2.36	3.64	7.05	0.80	0.80

[a] Orange model in Figure 3a.

[b] Blue (preferred) model in Figure 3a.

[c] Includes samples from the Namaqua-Natal Belt, green model in Figure 3a.

[d] Excludes samples from the Namaqua-Natal Belt.

[e] Quantiles computed for all granites including those without age estimates.

Table 2: Observed quantiles for heat-producing element concentrations at present used in modeling geotherm heat production at present and 3.5 Ga.

		Quantiles				
scenario[a]	HPE	0.05	0.25	0.50	0.75	0.95
	Recent (0.2 to 0 Ga)					
	K_2O (wt.%)	1.72	3.64	4.48	5.06	6.02
	Th (ppm)	2.70	9.56	17.1	27.6	49.3
	U (ppm)	0.79	2.30	4.24	6.92	16.0
A	A, present (μW m^{-3})	0.53	1.54	2.58	4.05	7.90
B	A, at 3.5 Ga (μW m^{-3})	1.86	4.72	7.35	10.53	19.76
	Archean (4.0 to 3.0 Ga)					
	K_2O (wt.%)	0.66	1.43	2.40	3.67	5.90
	Th (ppm)	0.59	3.10	5.55	10.5	22.3
	U (ppm)	0.22	0.54	1.10	2.29	7.74
C	A, present (μW m^{-3})	0.15	0.47	0.86	1.60	3.98
D	A, at 3.5 Ga (μW m^{-3})	0.62	1.52	2.73	4.80	11.25

[a]See Section 4.5.4 for details.

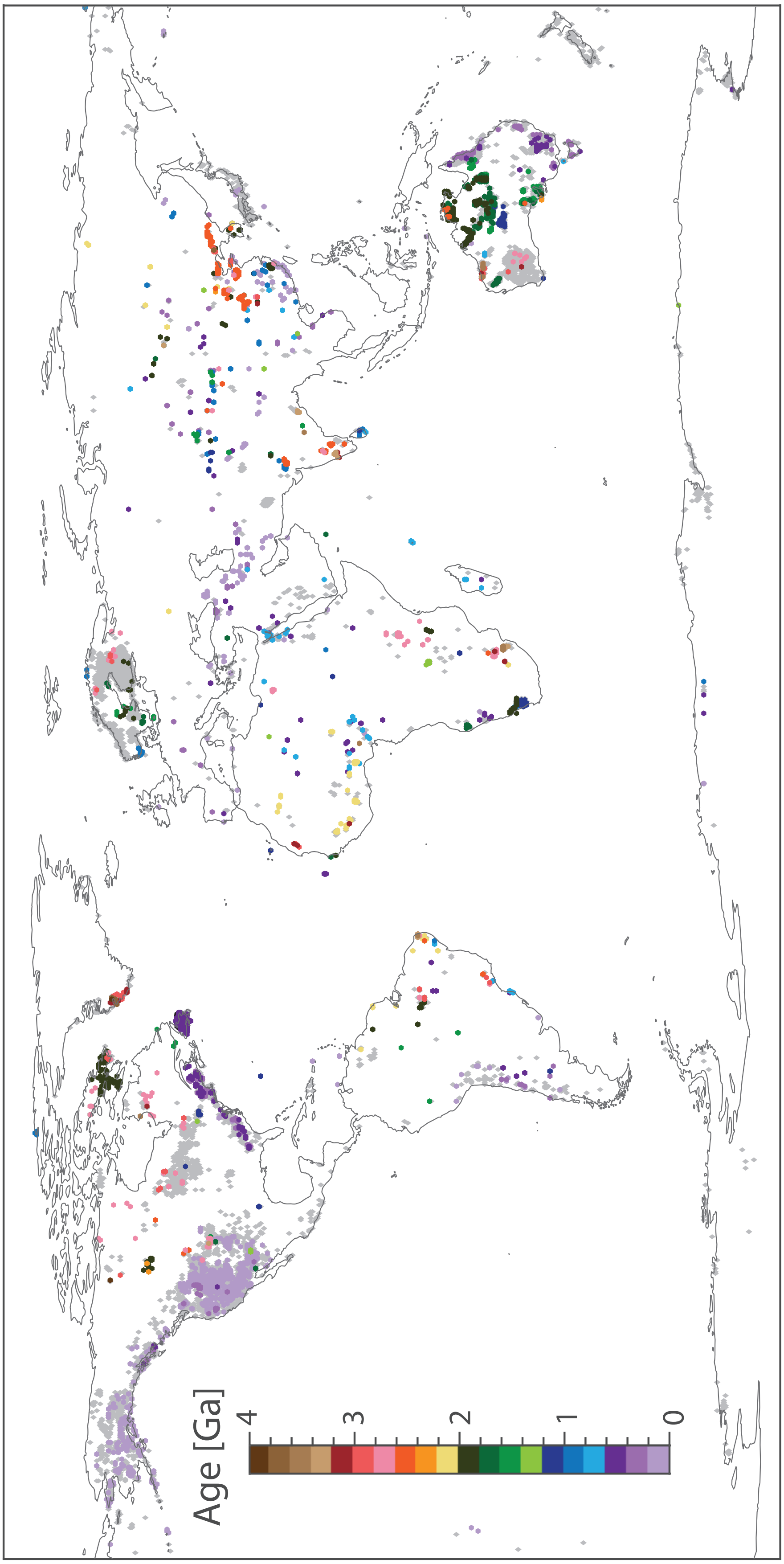

Figure 1: Temporal and spatial distribution of granites used in this study. Colored circles identify data with ages and open diamonds identify data without ages but used to explore statistical bias in the age dataset.

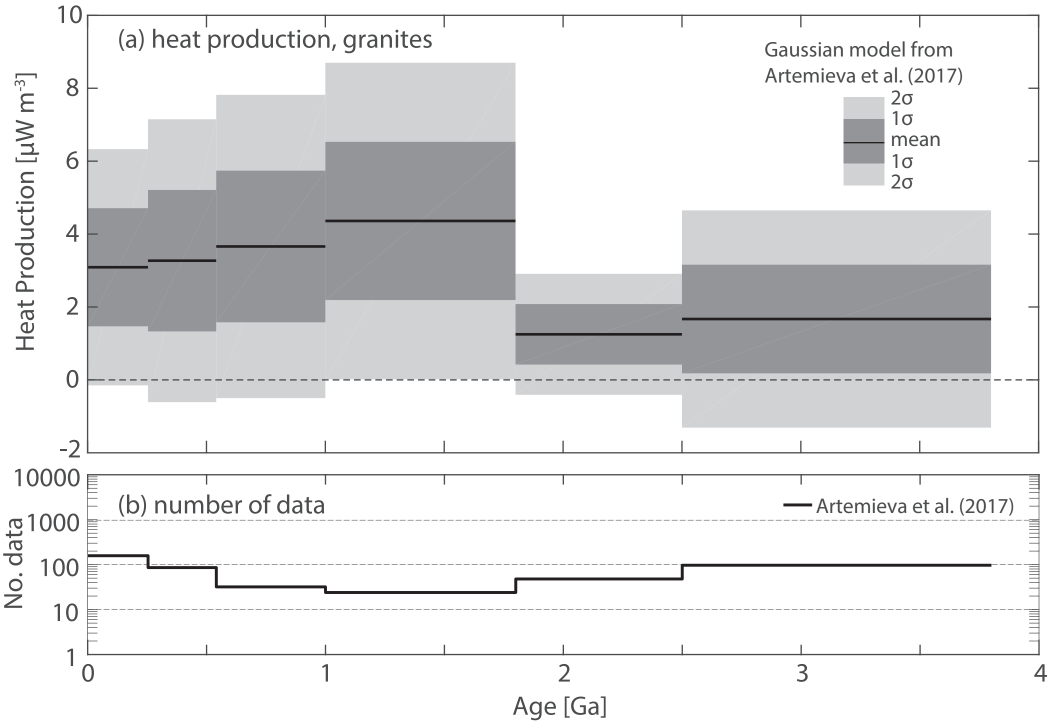

Figure 2: Granite heat production model by Artemieva et al. (2017) redrawn with reported Gaussian uncertainties. (a) Heat production of granites. Note the use of Gaussian uncertainties results in negative heat production estimates at -2σ from the mean for 5 of the 6 age bins. (b) Number of samples used to estimate the mean and standard deviations in (a).

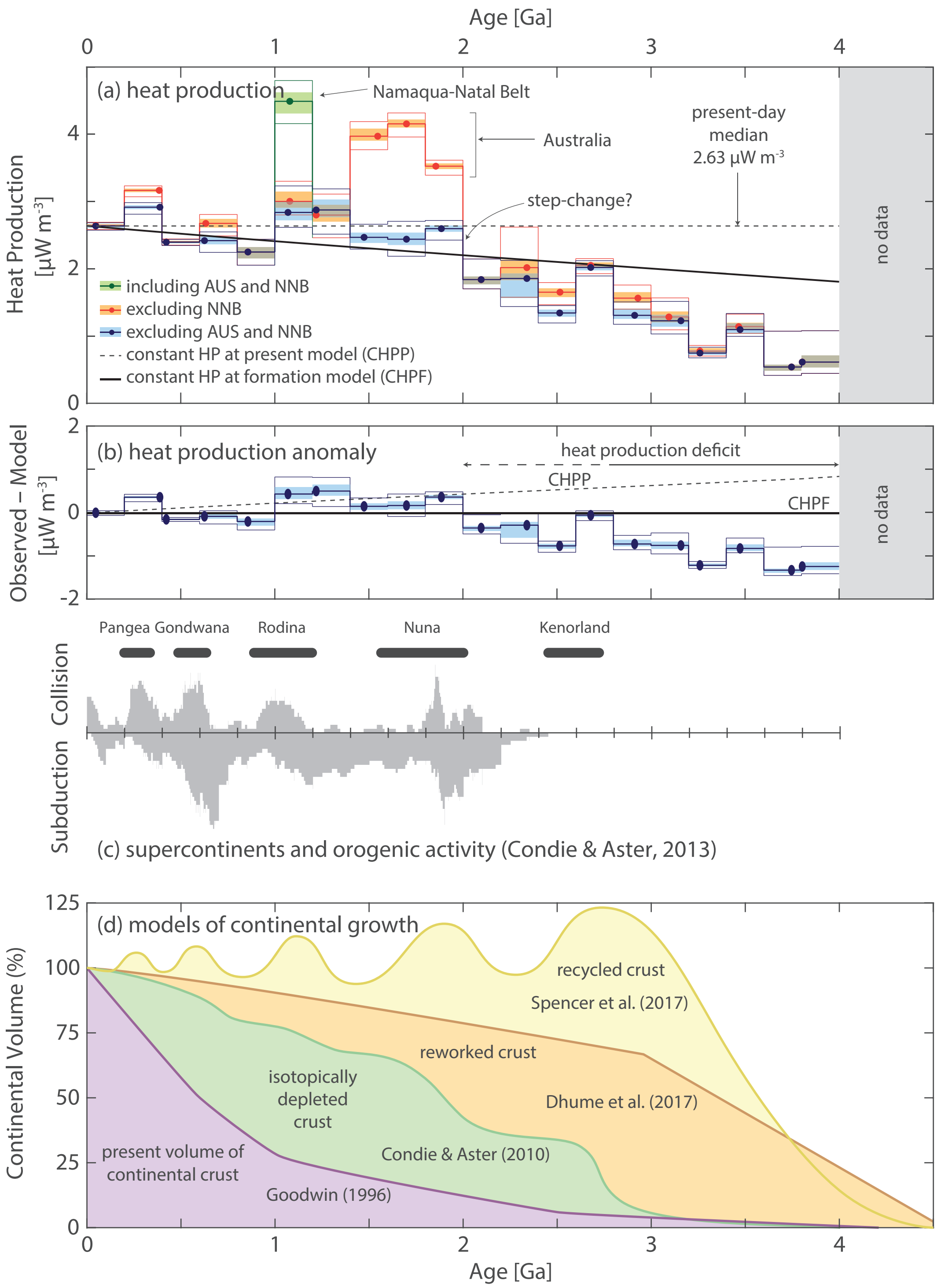

Figure 3: Granite heat production and continental crustal growth curves. (a) Global heat production estimates of granites as a function of formation age over the past 4 Ga estimated from present from K_2O, U and Th concentrations. Time series are estimated including samples: from Australia (AUS) and the Namaqua-Natal Belt (NNB, green), without NNB (orange), and without AUS and NNB (blue). The brown is created by an overlap of the orange and blue. The blue model is preferred because it considered the less geographically biased by anomalous high heat producing terranes. These models differ from Table 1 in that the uncertainty bounds are presented as the quantiles divided by the square-root of number of samples within each age bin. This uncertainty estimate gives an approximation analogous to 1- and 2-standard error confidence in the median heat production, providing a more accurate assessment of the uncertainty in the median. Two reference models for heat production are shown: (dashed black) constant heat production at present day (CHPP) regardless of the granite formation age; and (solid black) and constant heat production at formation (CHPF). Initial concentrations are chosen as the average for granites younger than 200 Ma: K_2O, Th, and U are 4.48 wt.%, 17.1 ppm and, 4.24 ppm, respectively. (b) The difference between the preferred global heat production model and CHPF model in (a). A global deficit in heat production exists in granites >2.0 Ga relative to the CHPF model. (c) The number of active collisional (above the line) and subduction orogens (below the line) active as a function of time (data from Condie and Aster, 2013). (d) Selected models of continental growth, figure updated and modified from (Spencer et al., 2017).

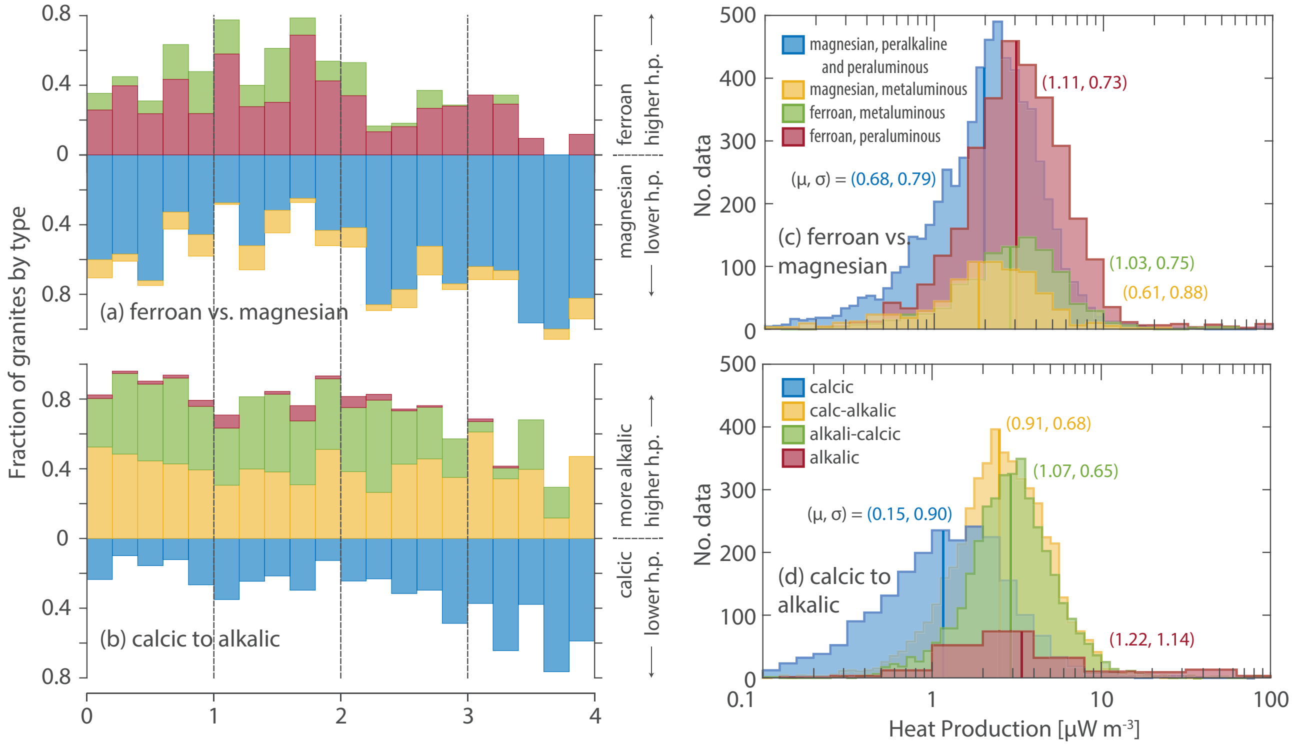

Figure 4: Composition and heat production of granites through time. The granite type is computed from major element chemistry using the classification by Frost et al. (2001). Australian and Namaqua-Natal Belt data are excluded from this analysis. (a) The normalized fraction of ferroan (red and green) and magnesian (blue and yellow) granites, color key in (c). (b) The normalized fraction of calcic to alkalic granites, color key in (d). (c) Heat production of ferroan and magnesian granites. (d) Heat production of calcic to alkalic granites.

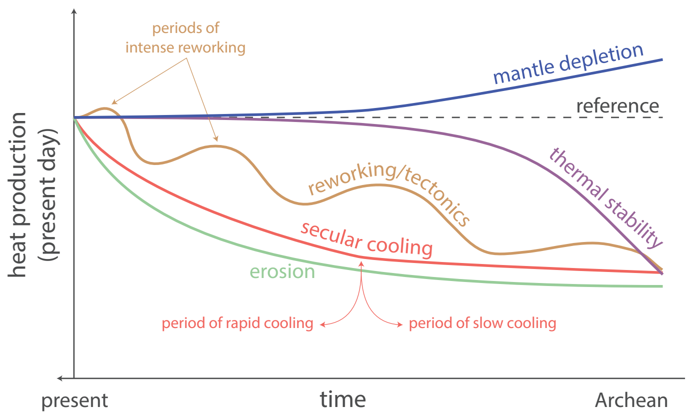

Figure 5: Hypothetical patterns of present-day variations in heat production expected as a result of time-varying global processes. All profiles are referenced to the average of recent granites. The reference curve assumes that all factors that generate granitic melts through time are free from other influences and therefore decay to yield a constant value with crystallization age. Relative magnitudes and exact timing of variations may be different and in reality, the true temporal heat production pattern may result from a combination of these processes.

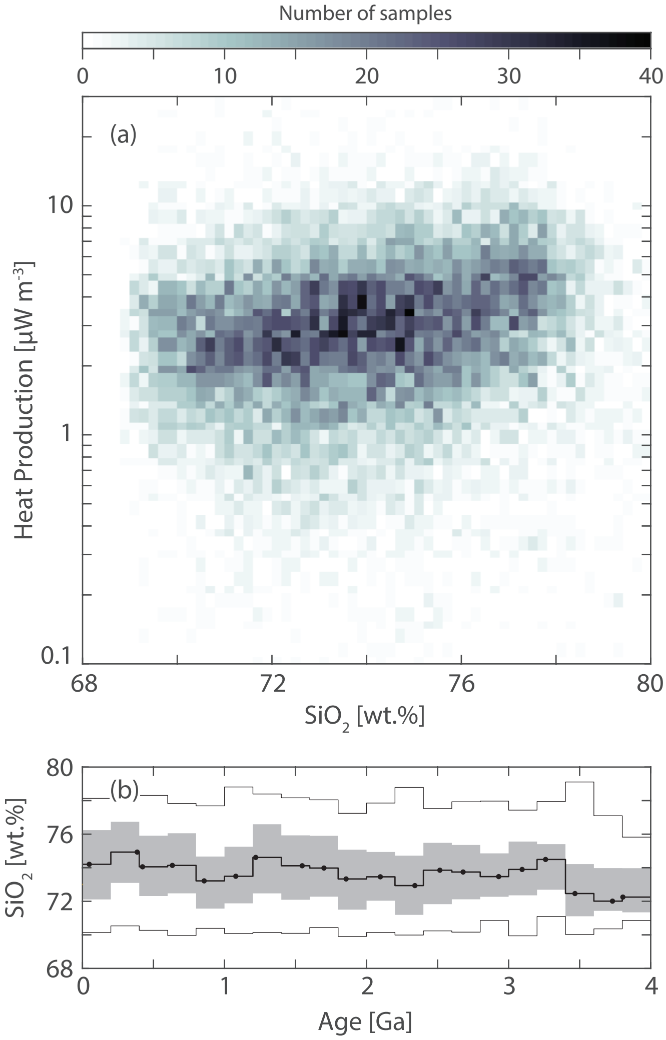

Figure 6: (a) Heat production of granites as a function of SiO_2. (b) SiO_2 variations with age.

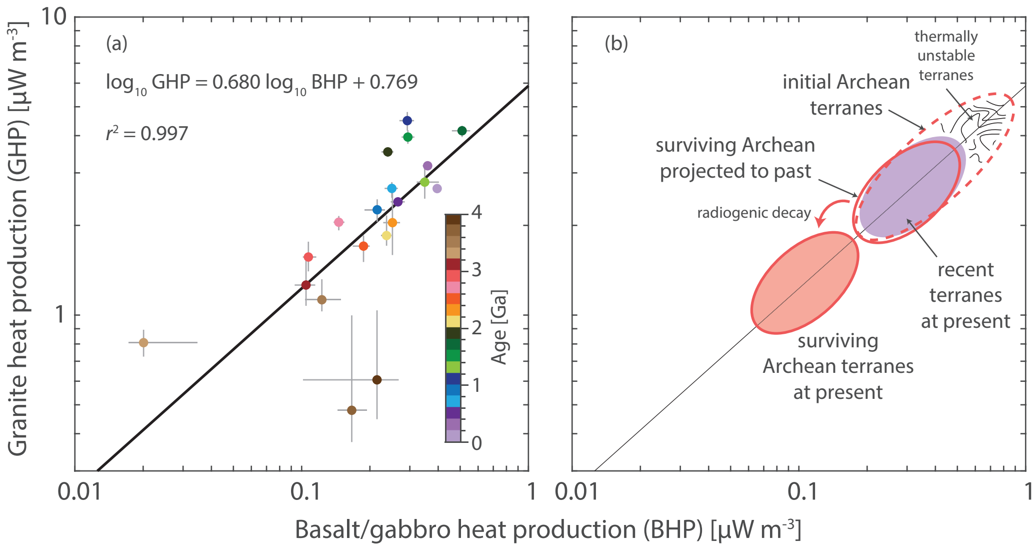

Figure 7: (a) The relationship between heat production of granites and basalt/gabbros with time. Each point identifies a 200 Ma age bin. Error bars represent the 5 and 95% quantiles divided by the square-root of the number of samples of each respective rock type. The equation given in the upper left describes the linear fit to the data (black line). (b) The effect of selective preservation and radioactive decay on the basalt/gabbro–granite heat production relationship. Initial Archean terranes with high heat production are thermally unstable and prone to reworking, melting, or tectonic destruction. The remaining Archean terranes may then yield a similar distribution in the Archean to present day granites and basalts before decaying to a lower heat production.

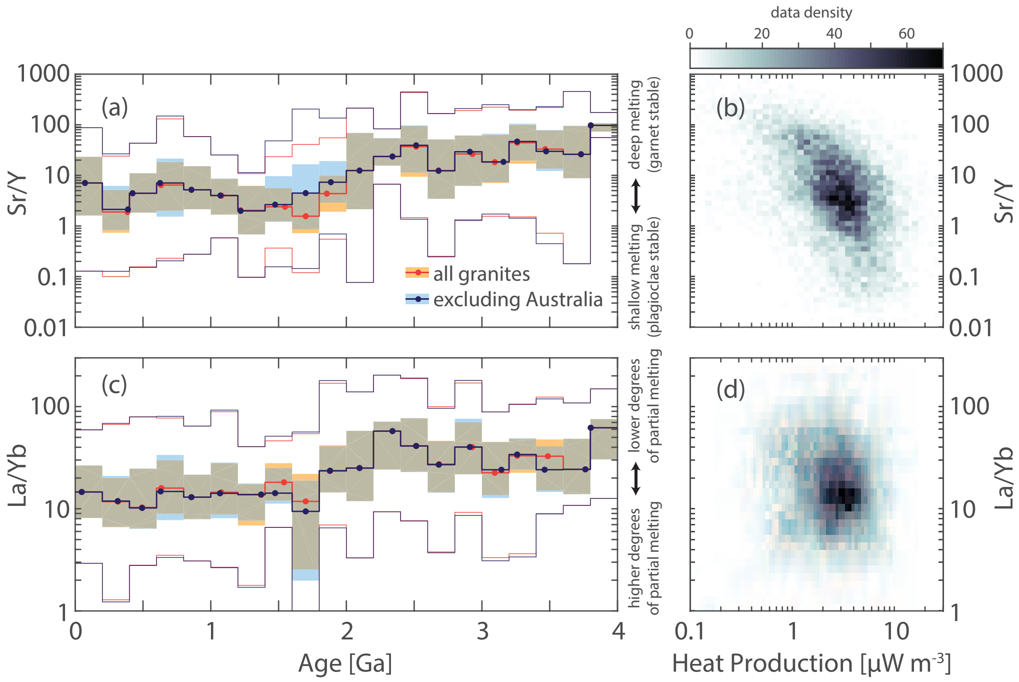

Figure 8: Chemical indicators that potentially reflect (a, b) the depth of melting (Sr/Y) and (c, d) the degree of partial melting and/or fractional crystallization (La/Yb) over the past 4 Ga.

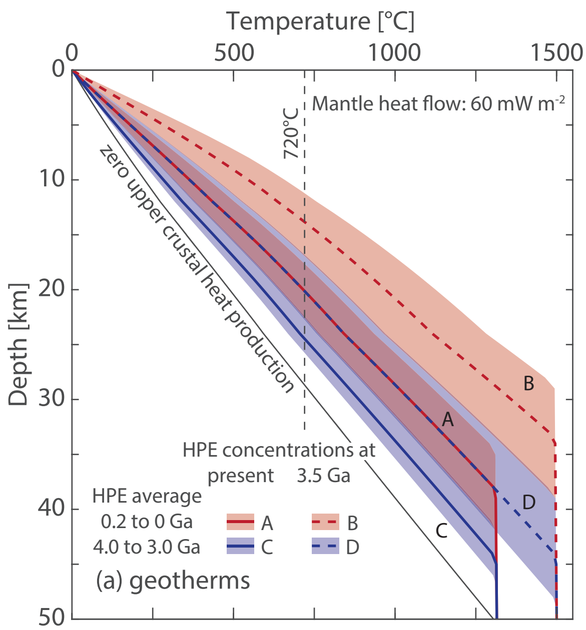

Figure 9: Geotherms computed using the array of granite heat production estimates at 4.0 to 3.0 Ga and 0.2 to 0 Ga. Crustal temperature scenarios for a mantle heat flow of 60 mW m^{-2}, approximating a distribution of rift geotherms with variable upper crustal heat production defined by four scenarios: (A) formation age 0.2 to 0 Ga at present; (B) formation age 0.2 to 0 Ma projected to 3.5 Ga; (C) formation age 4.0 to 3.0 Ga at present; and (D) 4.0 to 3.0 Ga projected to 3.5 Ga. A technical description of the geotherm parameters and computations are given in the Supplementary Material.

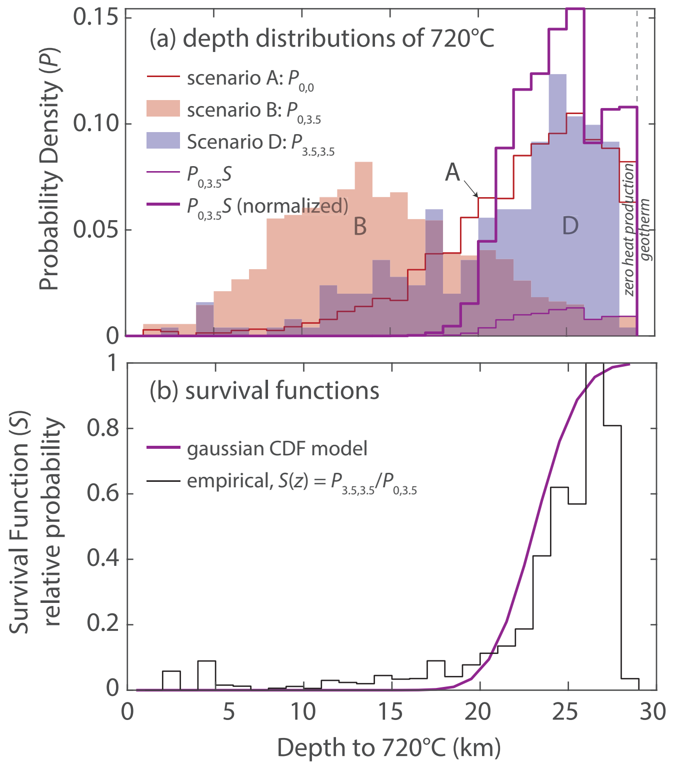

Figure 10: Selective preservation models for Archean crust. (a) The depth distribution of the 720°C isotherms in Figure 9: assuming a surface heat production defined by granites at present (scenario A, red line) and projected to 3.5 Ga (scenario B, filled red) and a surface heat production of Archean granites projected to 3.5 Ga (scenario D, filled blue). The temperature 720°C was chosen because it corresponds to the lower temperature limit for most granitic melts (Miller et al., 2003). The lines are computed by the product of the probability distribution B ($P_{0,3.5}$) and the best-fitting Gaussian CDF survival probability either unnormalized (light line) or normalized to an integrated PDF of 1 (heavy line). (b) Estimated survival functions using two methods: (heavy line) Gaussian CDF; and (light line) by dividing the distributions D by B ($P_{0,3.5}/P_{3.5,3.5}$) from (a). The best-fitting Gaussian CDF survival function has μ of 23.6 km and a σ of 2.0 km with a misfit of 0.29 μW m^{-3}. A more detailed description of the survival function is given in the Supplementary Material.